Alexandria Engineering Journal (2021) 60, 821–835

HOSTED BY

Alexandria University

Alexandria Engineering Journal

www.elsevier.com/locate/aej
www.sciencedirect.com

Impact of heated obstacle position on magneto-hybrid nanofluid flow in a lid-driven porous cavity with Cattaneo-Christov heat flux pattern

Shaik Jakeer [a], P. BalaAnki Reddy [a], A.M. Rashad [b], Hossam A. Nabwey [c,d,*]

[a] *Department of Mathematics, S.A.S., Vellore Institute of Technology, Vellore 632014, India*
[b] *Department of Mathematics, Faculty of Science, Aswan University, Aswan 81528, Egypt*
[c] *Department of Mathematics, College of Science and Humanities in Al-Kharj, Prince Sattam bin Abdulaziz University, Al-Kharj 11942, Saudi Arabia*
[d] *Department of Basic Engineering Science, Faculty of Engineering, Menoufia University, Shebin El-Kom 32511, Egypt*

Received 12 July 2020; revised 16 September 2020; accepted 7 October 2020
Available online 18 October 2020

KEYWORDS

Non-Darcy;
Porous medium;
Mixed convection;
Hartmann number;
Cu-Al_2O_3/water nanofluid;
Hot obstacle;
Lid-driven cavity;
Boussinesq approximations

Abstract This article mainly emphases on the study of magneto Cu-Al_2O_3/water hybrid nanofluid flow in a non-Darcy porous square cavity. The square geometry is a lid-driven enclosure with an inside heated square obstacle. Cattaneo-Christov heat flux pattern is used for the formulation of the heat equation. This type of problems may be applicable in the high temperatures in the different scientific processes, extrusion of polymers, aerodynamics extrusion and cooling hot glass. Dimensionless forms of governing flow expressions are computed numerically with Finite Volume Method via SIMPLER algorithm simultaneously. The characteristics of numerous dimensionless parameters such as; Richardson number ($0.1 \leqslant Ri \leqslant 100$), Hartmann number ($0 \leqslant Ha \leqslant 100$), height of hot square obstacle ($0.1 \leqslant H \leqslant 0.5$), width of hot square obstacle ($0.1 \leqslant W \leqslant 0.5$), Reynolds number ($0.1 \leqslant Re \leqslant 25$) and Darcy number $\left(10^{-2} \leqslant Da \leqslant 10^{-6}\right)$ are analyzed. The achieved results are projected graphically via streamlines, isotherms, local and average Nusselt numbers. The fluid flow and rate of heat transfer in the direction of the moving heated obstacle isfound to play an important role. The higher values of Ha decreases the local Nusselt number. Hybrid nanofluid provides a higher heat transfer rate than the nanofluids. Increasing the width of the obstacle cause to decline in the thickness of the right wall, this enhances the heat transfer in the clockwise direction.

1. Introduction

Nanofluids are a new class of fluids, contain nanosized solid particles (1–100 nm) in the ordinary liquid (water, lubricants,

* Corresponding author.
E-mail address: eng_hossam21@yahoo.com (H.A. Nabwey).
Peer review under responsibility of Faculty of Engineering, Alexandria University.

https://doi.org/10.1016/j.aej.2020.10.011

Nomenclature

D_1	position of the obstacle
W	width of the obstacle
H	height of the obstacle
L	length of enclosure
Ri	Richardson number
Re	Reynolds number
Ha	Hartmann number
DA	non-Darcy
Gr	Grashof number
C_p	specific heat
P	pressure (Nm^{-2})
B_0	magnetic field
Nu_s	local Nusselt number
Nu_m	average Nusselt number
k	thermal conductivity
Pr	Prandtl number
T	temperature
u	velocity component along x-direction (ms^{-1})
U	dimensionless velocity component along x-direction
U_0	lid velocity
V	dimensionless velocity component along y-direction
v	velocity component along y-direction ($m\ s^{-1}$)
x, y	Cartesian coordinates
X, Y	dimensionless Cartesian coordinates

Greek symbols

ρ	Density ($kg\ m^{-3}$)
μ	Dynamic viscosity ($kg\ m^{-1}\ s^{-1}$)
ν	Kinematic viscosity ($m^2 s^{-1}$)
σ	Electrical conductivity ($s\ m^{-1}$)
α	Thermal diffusivity ($m^2\ s^{-1}$)
λ	Cavity inclination angle
ε	Porosity

Subscripts

c	cold
hnf	Hybrid nanofluid
nf	nanofluid
bf	base fluid
f	fluid

Bio-fluids, oils polymer solutions) which was introduced by Choi [1]. In recent years nanofluids have received innovative procedures to enhance the rate of heat transfer in numerous applications such as mechanical industrial processes, domestic refrigerator, atomic reactors, fuel cells, energy storage systems [2–6] etc. Many researchers [7–10] studied the different types of nanoparticles with base fluids. Recently, many researchers are introduced hybrid nanofluid due to high heat transfer when compared to nanofluids. Hybrid nanofluid contains two types of nanoparticles suspended in a base fluid. The applications of hybrid nanofluids are solar water heating, transformers, heat exchangers, vehicle brake fluids, defense manufacturing, acoustics, microfluidics, microelectronics, transport, naval structures, propulsion, grinding and heat radiators. Mehryan et al. [11] studied the free convection of a Cu-Al_2O_3/water hybrid nanofluid and water-based Cu and Al_2O_3 nanofluid in a cavity. The Cu-Al_2O_3/water hybrid nanofluid gives the best results compared Al_2O_3 nanoparticles. Giwa et al. [12] analyzed the hybrid nanofluids have to improve the thermal and flow properties of the base fluid which consequently enhanced the free convection behavior of Cu-water and $MWCNT$-water nanofluids in a cavity. A number of investigations on the influence of nanoparticle use have been cited in the research [13–16].

Mixed convective flow in a lid-driven square cavity plays a significant attention in view of its extensive range of applications in many engineering and technological areas, such as heat exchanger devices, cooling of electronic devices and MEMS, thermal insulation, petroleum reservoirs, oil extraction, solid matrix heat exchangers, geothermal and geophysical engineering, chemical catalytic reactors and processes, geothermal systems and storage of nuclear waste materials [17–27] etc. Manchanda et al. [28]. Analyzed the natural and forced convection flows numerically in a two-sided lid-driven square cavity with a heated triangle obstacle. Gangawane [29] investigated the magneto hydrodynamic free convection of an open-ended square cavity in the effect of the angle of a magnetic field and different heater locations. Also Fluid flow through porous media has a wide range of applications in scientific and engineering activity which includes such diverse fields as soil mechanics, thermal and acoustic insulation efficiency, filtration, heat removal from nuclear fuel debris, petroleum engineering, transpiration cooling, use of electrochemical fuel cell devices, lithium-ion batterie. Darcy's law depicts the conduct of fluid flows in porous media. According to the Darcy's law, the pressure gradient in the porous media is linearly proportional to the velocity of the fluid. Non-Darcy behavior is significant for describing fluid flow in porous media in a context where high velocity occurs. Raizah and Aly [15] numerically studied the natural convection of Cu–water nanofluids from a heated complex shape in a cavity with the effect of a partially layered non-Darcy porous medium. Alsabery et al. [30] numerically studied the fluid flow and heat transfer in a square non-Darcy porous cavity containing a central square solid body. Krishna et al. [31] used the finite volume method to investigate the natural convection in a non-Darcy anisotropic porous cavity. Sheikholeslami and Sadoughi [32] presented the magneto hydrodynamic CuO-H_2onanofluid flow inside a porous cavity having four obstacles. Merrikh and Mohamad [33] investigated the Darcy effect in natural convection flow in an enclosure filled with vertically two layers of porous media. Kefayati [34] considered the Finite Difference Lattice Boltzmann method (FDLBM) to study mixed convection in a lids-driven square cavity for more details see [35,36].

The investigation of a magnetic parameter has incredible properties on convective and heat transfer. A magnetic parameter is significant in science and industrial applications such as cooling of different metals, metal coating, reactor cooling,

purification of liquid metals, molten polymers, glass industry, chemical engineering, and magneto hydrodynamic electrical power generator, etc. Convective and heat transfer control can be accomplished by the use of magnetic field effects in many experiments, such as applications for cavity flow, jet flow applications, separate flow and many others [37–41]. Sheikholeslami and Rashidi [42] studied the natural convection nanofluid (Fe_3O_4–water) flow in the presence of the magnetic field, volume fraction and Rayleigh number lead to an increase of the local Nusselt number. Hosseinzadeh et al. [43] investigated the cross-fluid nanofluid flow considering the nanoparticles and gyrotactic microorganisms over a three-dimensional cylinder under the influence of the magnetic field. Bourantas and Loukopoulos [44] studied the effects of temperature dependent properties of the natural convection flow in an inclined square cavity filled with micropolar-nanofluid (Al_2O_3 -water) under the influence of a magnetic field.

The heat transfer phenomenon has remarkable attention because of its various applications in numerous fields of industry and science, such type of applications includes extrusion of polymers, aerodynamics extrusion, molten polymers, the high temperatures in the different scientific processes, cooling of the glass sheet plays a significant role. Fourier's law stated to Fourier's model a thermal relaxation time factor to increase heat transfer but it is difficult for different materials to relax in different thermal periods. In view of this fact, Christov [45] was established for the efficient heat transfer mechanism by the derivative model, then it is called the Cattaneo-Christov heat flux model.

The main intention of the present research is to study the numerical analysis of the heated obstacle position on magneto-hybrid nanofluid flow in a lid-driven porous cavity with Cattaneo-Christov heat flux pattern. To the best of author's knowledge and based on the above literature survey, no studies have reported on hybrid nanofluid flow in a lid-driven non-darcy porous cavity with Cattaneo-Christov heat flux Pattern. In addition, it attempts to describe the impact of various parameters on the flow and heat transfer. The obtained results are validated with previous numerical investigations and the effect of the significant parameters (Hartmann number, non-Darcy, Richardson number, Reynolds number, and hybrid nanofluid) on the fluid flow and heat are researched. The obtained results are presented via graphically in the form of streamlines, isotherms, local Nusselt number, and average Nusselt number.

2. Mathematical formulation

We considered steady 2Dmixed convective flow of water-based nanofluid (Cu or Al_2O_3)/ hybrid nanofluid (Cu-Al_2O_3) in a lid-driven cavity and a schematic view of the problem is displayed in Fig. 1. The Newtonian fluid flow is considered as incompressible and laminar. In addition, the attribute of viscous dissipation is neglected. The right vertical wall is considered as a heat sink (T_c) and the remaining walls (top, bottom, and left) are treated as adiabatic. A heated square obstacle (T_h) placed at the bottom of the square cavity. Here L and W are indicated the length and width of the cavity and obstacle, respectively. The distance between the heated square obstacle and the left wall of the cavity is $D1$. Table1 Shows the thermophysical properties of two different nanoparticles and the base fluid. The Boussinesq approximation is consistent with the following governing equations [46–48].

$$\frac{\partial u}{\partial x}+\frac{\partial v}{\partial y}=0, \tag{1}$$

$$u\frac{\partial u}{\partial x}+v\frac{\partial u}{\partial y}=-\frac{1}{\rho_{hnf}}\frac{\partial p}{\partial x}+\upsilon_{hnf}\left(\frac{\partial^2 u}{\partial x^2}+\frac{\partial^2 u}{\partial y^2}\right)+\frac{\sigma_{hnf}B_0^2}{\rho_{hnf}}\left(v\sin\Phi\cos\Phi-u\sin^2\Phi\right) -\frac{\upsilon_{hnf}}{K}u-\frac{F_r}{\sqrt{K}}u\sqrt{u^2+v^2} \tag{2}$$

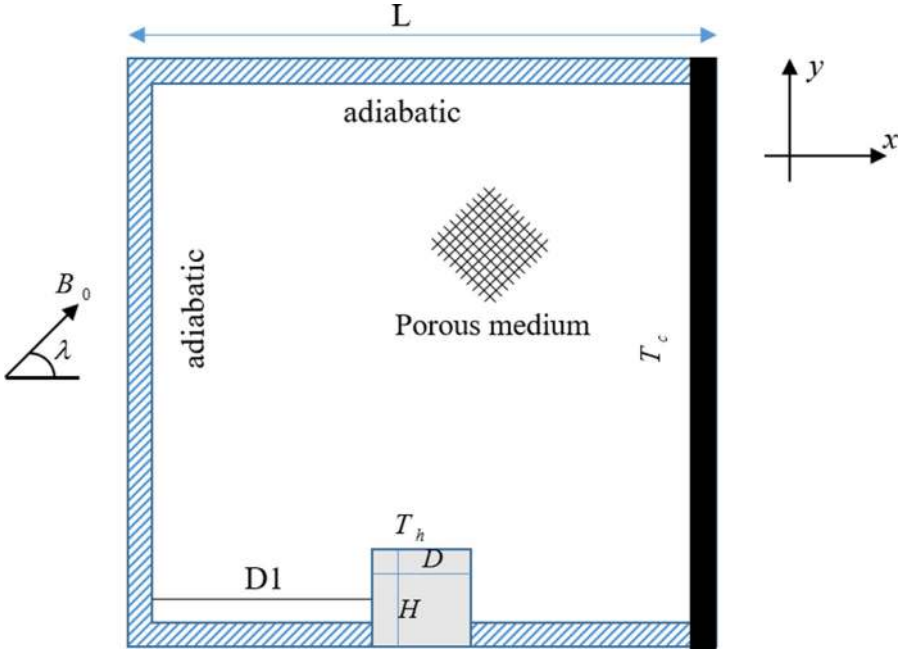

Fig. 1 Configuration of geometry.

Table 1 Thermophysical properties of H_2O, Cu, and Al_2O_3(by Rashad [49]).

Physical properties	Water (H_2O)	Copper (Cu)	Alumina (Al_2O_3)
$k\left(\mathrm{W}\times(\mathrm{m\ K})^{-1}\right)$	0.613	401	40
$C_p\left((\mathrm{kgK})^{-1}\times\mathrm{J}\right)$	4179	385	765
$\rho\left(\mathrm{kg}\times\mathrm{m}^{-3}\right)$	997.1	8933	3970
$\sigma(\mu\mathrm{s}\times\mathrm{cm}^{-1})$	0.05	5.96×10^{7}	1×10^{-10}
$\beta_T\times\frac{1}{\mathrm{K}}\times10^{-5}$	21	1.67	0.85

$$u\frac{\partial v}{\partial x}+v\frac{\partial v}{\partial y}=-\frac{1}{\rho_{hnf}}\frac{\partial p}{\partial y}+\upsilon_{hnf}\left(\frac{\partial^2 v}{\partial x^2}+\frac{\partial^2 v}{\partial y^2}\right)+g\beta_{hnf}(T-T_c)+\frac{\sigma_{hnf}B_0^2}{\rho_{hnf}}(u\sin\Phi\cos\Phi-v\cos^2\Phi)-\frac{\upsilon_{hnf}}{K}v-\frac{F^*}{\sqrt{K}}v\sqrt{u^2+v^2} \tag{3}$$

$$\left(\rho c_p\right)_{hnf}\left(u\frac{\partial T}{\partial x}+v\frac{\partial T}{\partial y}\right)=k_{hnf}\left(\frac{\partial^2 T}{\partial x^2}+\frac{\partial^2 T}{\partial y^2}\right)-\delta_e\left(u\frac{\partial u}{\partial x}\frac{\partial T}{\partial x}+v\frac{\partial v}{\partial y}\frac{\partial T}{\partial y}+u^2\frac{\partial^2 T}{\partial x^2}+v^2\frac{\partial^2 T}{\partial y^2}+2uv\frac{\partial^2 T}{\partial x\partial y}+u\frac{\partial v}{\partial x}\frac{\partial T}{\partial y}+v\frac{\partial u}{\partial y}\frac{\partial T}{\partial x}\right) \tag{4}$$

In above u and v are velocity component along x and y-direction, T is the temperature, p is the pressure, k is the thermal conductivity, B_0 is the magnetic field, x, y are the Cartesian coordinates, $\rho$is the Density, $\sigma$is the Electrical conductivity, v is the Kinematic viscosity, F^* is the Forchheimer coefficient, K is the permeability.

The following dimensionless parameters are used to modernize the governing equations as dimensionless:

Table 2 Comparisons of local Nusselt number at the upper wall for the case of Pr = 0.71, Gr = 10^2.

Re	100	400	1000
Khanafer and Chamkha [33]	1.94	3.84	6.33
Iwatsu et al. [34]	2.01	3.91	6.33
Present data	1.93	3.91	6.31

$$X=\frac{x}{L},\ U=\frac{u}{U_0},\ P=\frac{p}{\rho_{hnf}U_0^2},\ Y=\frac{y}{L},\ V=\frac{v}{U_0},\ \theta=\frac{T-T_c}{T_h-T_c},$$

By using dimensionless parameters, Eqs. (1)–(4) rehabilitated as:

$$\frac{\partial U}{\partial X}+\frac{\partial V}{\partial Y}=0, \tag{6}$$

$$U\frac{\partial U}{\partial X}+V\frac{\partial U}{\partial Y}=-\frac{\partial P}{\partial X}+\frac{\nu_{hnf}}{\nu_f}\frac{1}{Re}\left(\frac{\partial^2 U}{\partial X^2}+\frac{\partial^2 U}{\partial Y^2}\right)+\frac{Ha^2}{\frac{\rho_{hnf}}{\rho_f}}\frac{1}{Re}(V\sin\Phi\cos\Phi-U\sin^2\Phi)-\frac{\nu_{hnf}}{\nu_{hnf}}\frac{1}{Re}\frac{U}{Da}-\frac{F^*}{\sqrt{Da}}U\sqrt{U^2+V^2} \tag{7}$$

$$U\frac{\partial V}{\partial X}+V\frac{\partial V}{\partial Y}=-\frac{\partial P}{\partial Y}+\frac{\nu_{hnf}}{\nu_f}\frac{1}{Re}\left(\frac{\partial^2 V}{\partial X^2}+\frac{\partial^2 V}{\partial Y^2}\right)+Ri\frac{\beta_{hnf}}{\beta_f}\theta+\frac{Ha^2}{\frac{\rho_{hnf}}{\rho_f}}\frac{1}{Re}(U\sin\Phi\cos\Phi-V\cos^2\Phi)-\frac{\nu_{hnf}}{\nu_{hnf}}\frac{1}{Re}\frac{V}{Da}-\frac{F^*}{\sqrt{Da}}V\sqrt{U^2+V^2} \tag{8}$$

$$\left(U\frac{\partial\theta}{\partial X}+V\frac{\partial\theta}{\partial Y}\right)=\frac{\alpha_{hnf}}{\alpha_f}\frac{1}{\mathrm{Pr}}\frac{1}{Re}\left(\frac{\partial^2\theta}{\partial X^2}+\frac{\partial^2\theta}{\partial Y^2}\right)-\gamma_e\left(U\frac{\partial V}{\partial X}\frac{\partial\theta}{\partial Y}+V\frac{\partial U}{\partial Y}\frac{\partial\theta}{\partial X}+U^2\frac{\partial^2\theta}{\partial X^2}+V^2\frac{\partial^2\theta}{\partial Y^2}+2UV\frac{\partial^2\theta}{\partial X\partial Y}+U\frac{\partial U}{\partial X}\frac{\partial\theta}{\partial X}+V\frac{\partial V}{\partial Y}\frac{\partial\theta}{\partial Y}\right) \tag{9}$$

where

$Gr=\frac{g\beta_f\Delta T\,L^3}{\nu_f^2}$, $Re=\frac{U_0\,L}{\nu_f}$, $Ri=\frac{Gr}{Re^2}$, $Ha=B_0\,L\sqrt{\frac{\sigma_f}{\rho_f\nu_f}}$, $Da=\frac{K}{L^2}$, $\mathrm{Pr}=\frac{\nu_f}{\alpha_f}$.

The appropriate initial and boundary conditions over the walls of the cavity are as follows:

$$\begin{aligned}&Y=0,\ 0\leqslant X\leqslant 1,\ U=0,\ V=0,\ \frac{\partial\theta}{\partial Y}=0,\\&Y=1,\ 0\leqslant X\leqslant 1,\ U=1,\ V=0,\ \frac{\partial\theta}{\partial Y}=0,\end{aligned} \tag{10}$$

$$\begin{aligned}&X=0,\ 0\leqslant Y\leqslant 1,\ U=0,\ V=0,\ \frac{\partial\theta}{\partial X}=0,\\&X=1,\ 0\leqslant Y\leqslant 1,\ U=\ 0,\ V=0,\ \theta=0,\end{aligned} \tag{11}$$

Hot obstacle boundary conditions are as:

$$\begin{aligned}&X-D1=0\,\&\,0\leqslant Y\leqslant H\rightarrow\{\theta=1,\ 0\leqslant(X,Y)\leqslant 1\\&X-(D+D1)=0\,\&\,0\leqslant Y\leqslant H\rightarrow\{\theta=1,\ 0\leqslant(X,Y)\leqslant 1\\&\text{and}\\&Y-H=0\text{ and }0\leqslant X-D1\leqslant D\rightarrow\{\theta=1,\ 0\leqslant(X,Y)\leqslant 1\end{aligned} \tag{12}$$

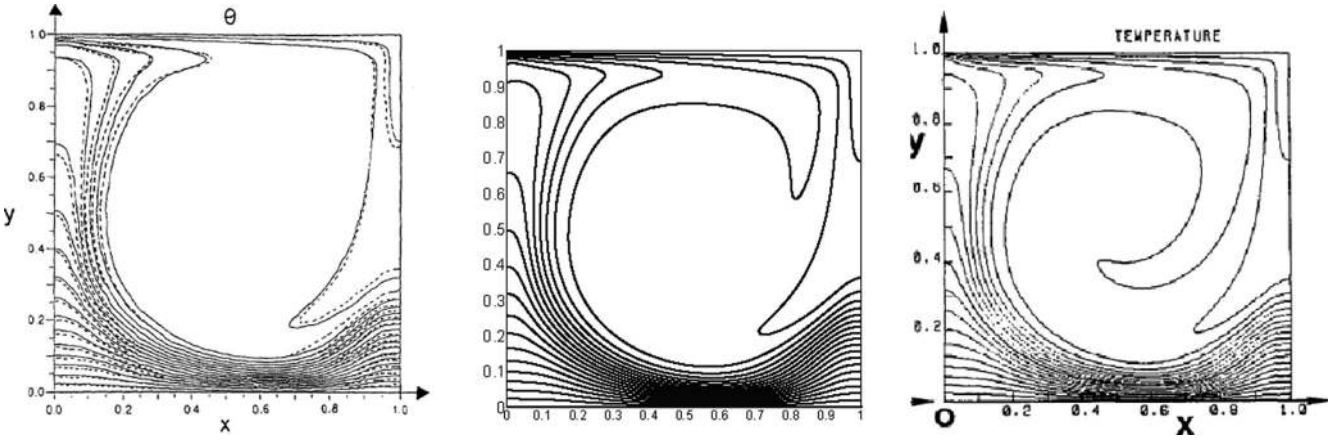

Fig. 2 Figure comparison with Refs.[43] and [44].

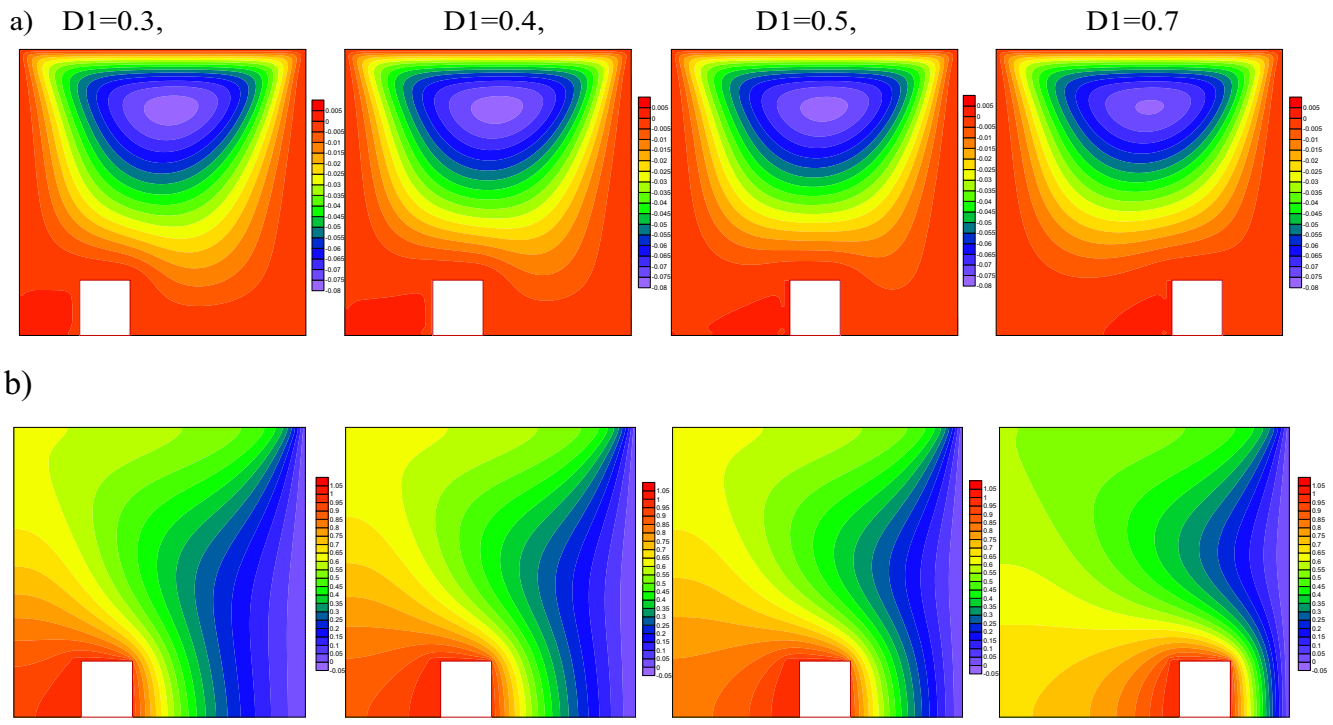

Fig. 3 Various values of D1 on streamlines (top) and isothermal (bottom).

2.1. The local Nusselt number

The local Nusselt number along hot obstacle is as:

$$Nu_v = -\left(\frac{k_{hnf}}{k_f}\right)\left(\frac{\partial\theta}{\partial X}\right) \tag{13}$$

Or

$$Nu_h = -\left(\frac{k_{hnf}}{k_f}\right)\left(\frac{\partial\theta}{\partial Y}\right)$$

The average Nusselt number of hot obstacle is obtained the integrating the Eq.13 (local Nusselt number of hot obstacle) as follows (by Esfe [47]):

$$Nu = \int_{\text{Hot obstacle}} Nu_H dX\Big|_{Y=H} + \int_{\text{Hot obstacle}} Nu_v dY\Big|_{X=D1+D} + \int_{\text{Hot obstacle}} Nu_v dY\Big|_{X=D1} \tag{14}$$

The mathematical expressions of μ_{hnf}, k_{hnf},$(c_p)_{hnf}$, $(\beta_T)_{hnf}$, σ_{hnf}, and ρ_{hnf} areas follows (by Rashad [49]):

Thermal diffusivity of the hybrid nanofluid is follows as:

$$\alpha_{hnf} = \frac{k_{hnf}}{(\rho c_p)_{hnf}}, \tag{15}$$

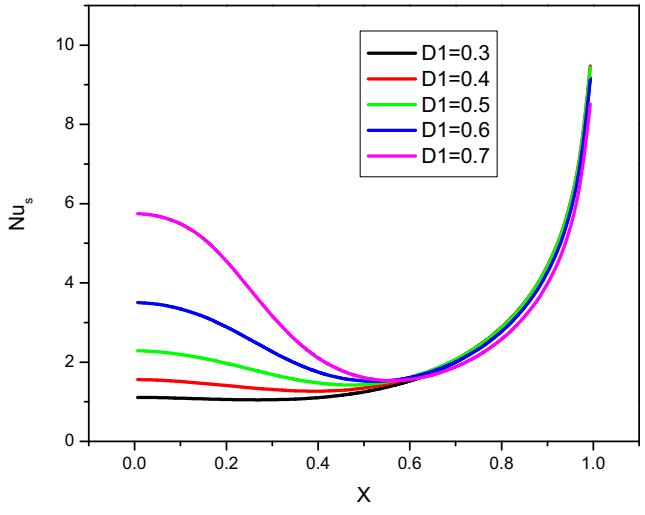

Fig. 4 The effect ofD1on the local Nusselt.

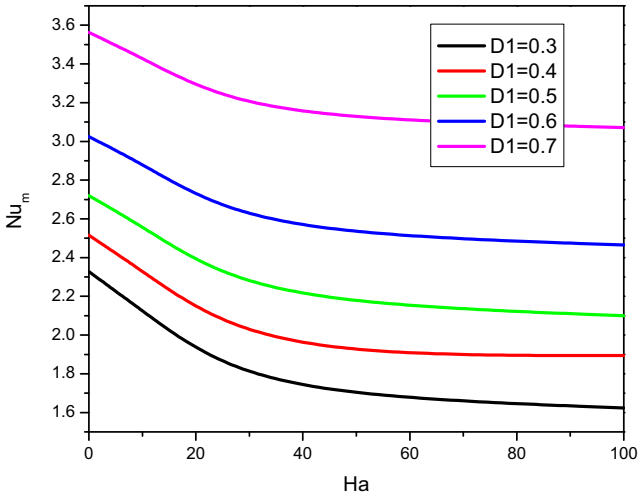

Fig. 5 Variationof D1 on the average Nusselt number.

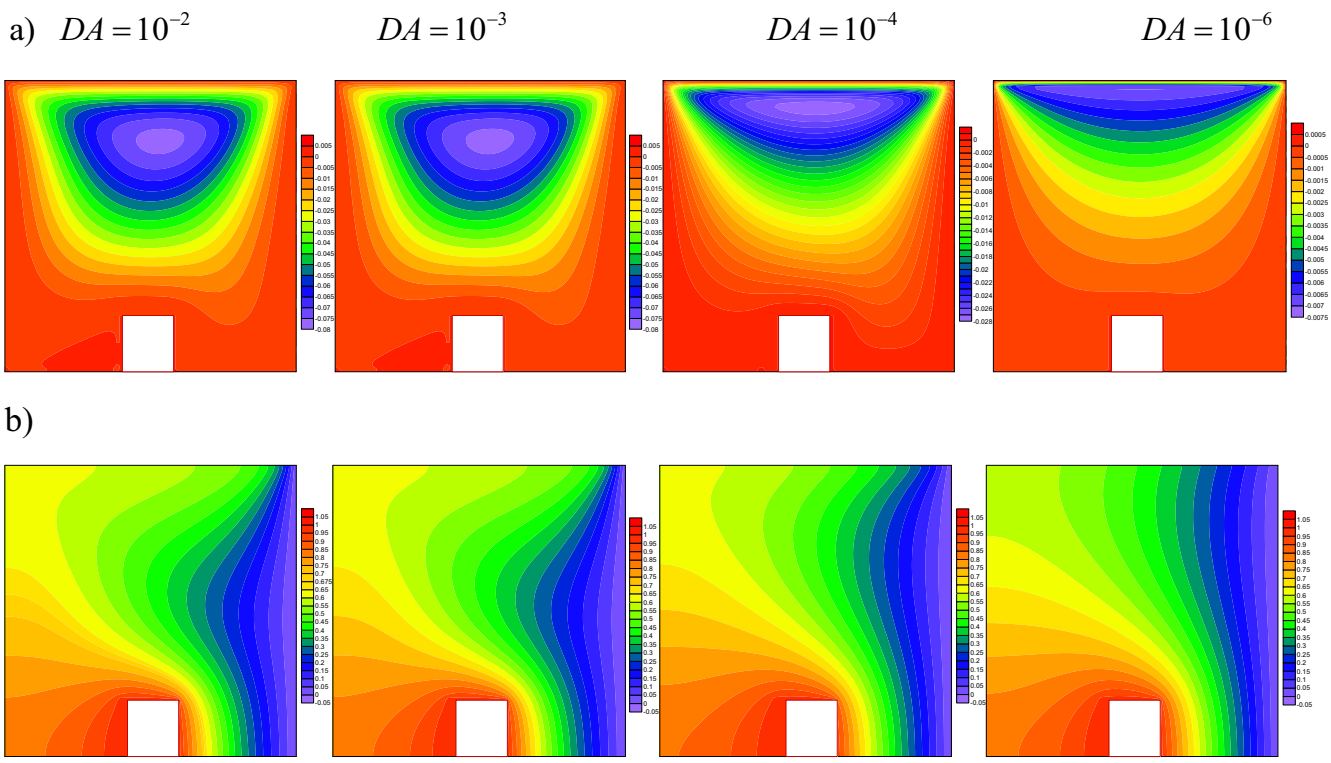

Fig. 6 Various values of DA on streamlines (top) and isothermal (bottom).

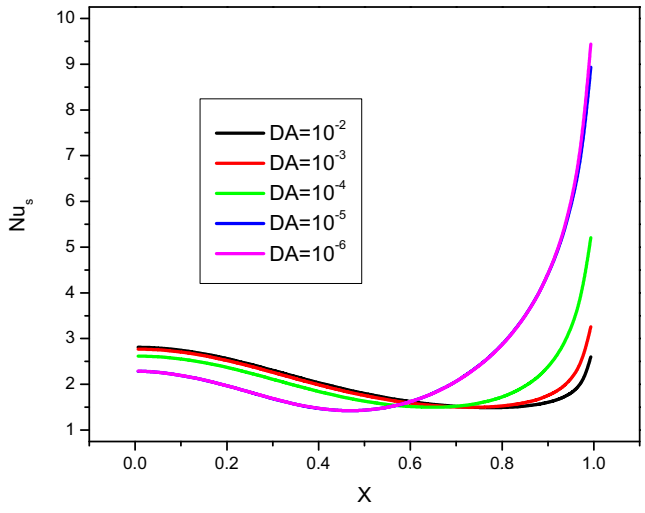

Fig. 7 The effect of DA on the local Nusselt number.

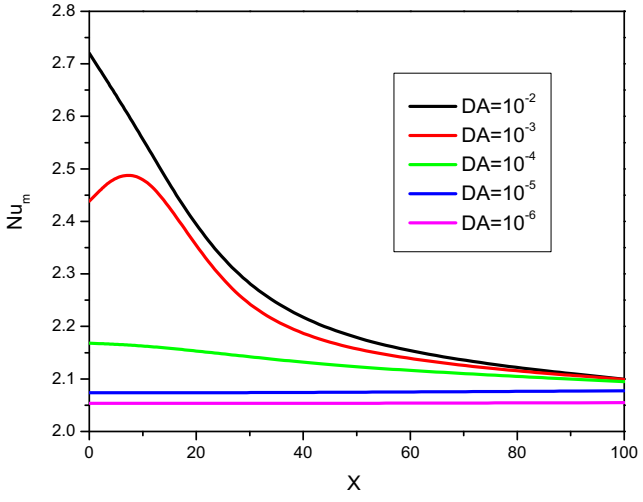

Fig. 8 The effect of DA on the average Nusselt number.

Effective density of the hybrid nanofluid is expressed as:

$$\rho_{hnf} = \phi_{Al_2o_3}\rho_{Al_2o_3} + \phi_{Cu}\rho_{Cu} + (1-\phi)\rho_{bf}, \tag{16}$$

The heat capacitance of the hybrid nanofluid is expressed as:

$$\left(\rho C_p\right)_{hnf} = \phi_{Al_2o_3}\left(\rho C_p\right)_{Al_2o_3} + \phi_{Cu}\left(\rho C_p\right)_{Cu} + (1-\phi)\left(\rho C_p\right)_{bf} \tag{17}$$

The thermal conductivity of hybrid nanofluid is expressed as:

$$\frac{k_{hnf}}{k_{bf}} = \frac{\left(\frac{\left(\phi_{Al_2o_3}k_{Al_2o_3}+\phi_{Cu}k_{Cu}\right)}{\phi} + 2k_{bf} + 2\left(\phi_{Al_2o_3}k_{Al_2o_3} + \phi_{Cu}k_{Cu}\right) - 2\phi k_{bf}\right)}{\left(\frac{\left(\phi_{Al_2o_3}k_{Al_2o_3}+\phi_{Cu}k_{Cu}\right)}{\phi} + 2k_{bf} - \left(\phi_{Al_2o_3}k_{Al_2o_3} + \phi_{Cu}k_{Cu}\right) + \phi k_{bf}\right)}. \tag{18}$$

The effective dynamic viscosity of the hybrid nanofluid is expressed as:

$$\mu_{hnf} = \frac{\mu_{bf}}{\left(1-\left(\phi_{Al_2o_3}+\phi_{Cu}\right)\right)^{2.5}}. \tag{19}$$

The effective electrical conductivityof the hybrid nanofluid is expressed as:

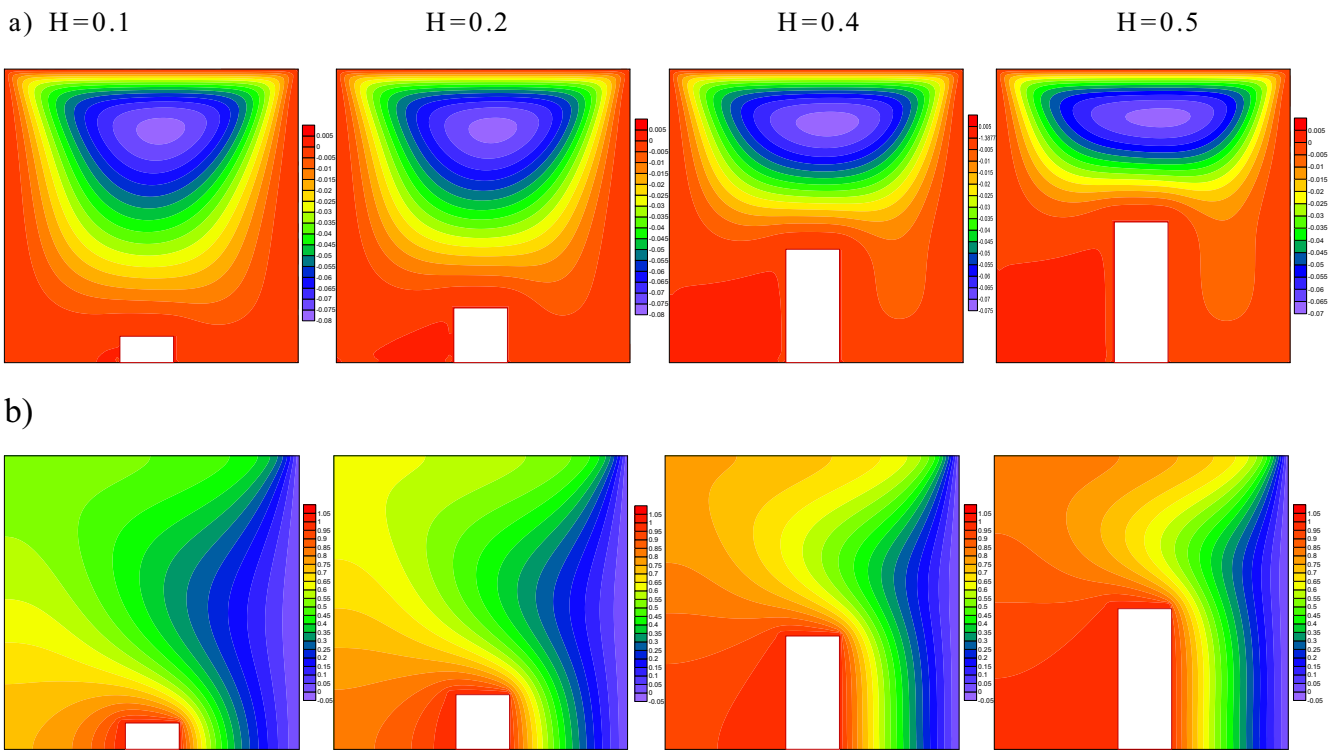

Fig. 9 Various values of H on streamlines (top) and isothermal (bottom).

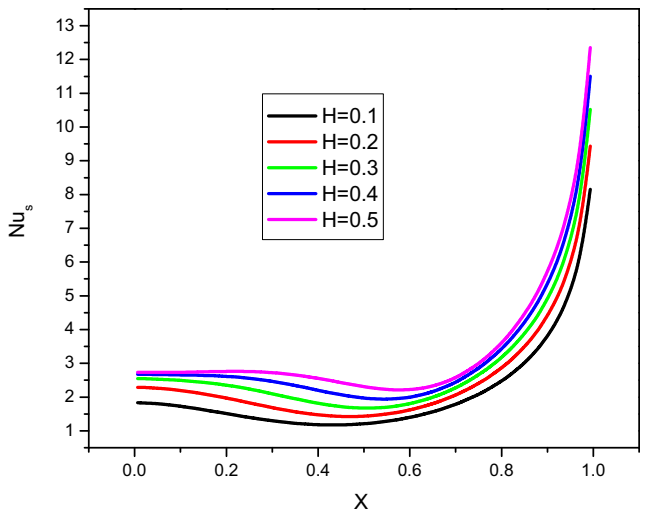

Fig. 10 The effect of H on the local Nusselt number.

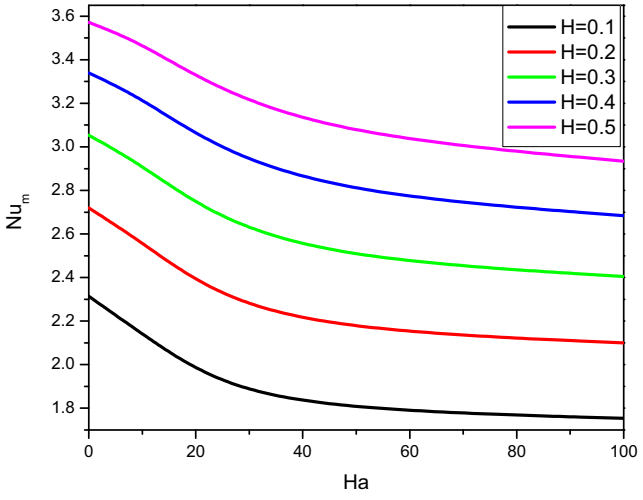

Fig. 11 The effect ofH on the average Nusselt number.

$$\frac{\sigma_{hnf}}{\sigma_{bf}} = 1 + \frac{3\left(\frac{\left(\phi_{Al_2o_3}\sigma_{Al_2o_3}+\phi_{Cu}\sigma_{Cu}\right)}{\sigma_{bf}} - \left(\phi_{Al_2o_3}+\phi_{Cu}\right)\right)}{\left(\frac{\left(\phi_{Al_2o_3}\sigma_{Al_2o_3}+\phi_{Cu}\sigma_{Cu}\right)}{\phi\sigma_{bf}} + 2\right) - \left(\frac{\left(\phi_{Al_2o_3}\sigma_{Al_2o_3}+\phi_{Cu}\sigma_{Cu}\right)}{\sigma_{bf}} - \left(\phi_{Al_2o_3}+\phi_{Cu}\right)\right)} \tag{20}$$

3. Numerical method and validation

Finite volume-based simple algorithm has been used to compute the governing Eqs. (6)–(9) withthe appropriateboundary conditions (10)–(13). To solve the convective and the diffusion-terms, we employed an upwind and central difference schemes. In order to obtain a result, the square cavity was meshed by 81×81 and residual convergence has fixed as 10^{-5}. To validate the obtained numerical results, the outcome are compared with the earlier work of Refs. [50,51] in some specific values of *Gr* and *Re*which is exhibits in Table 2. It is observed that the outcome of present results, Refs. [50,51] results are in good agreement. It is also observed from Fig. 2, present result isotherms and earlier work of Khanafer and Chamkha [50] and Iwatsu et al. [51] isotherms' are similar. This is revealed that the outcomes results are precious.

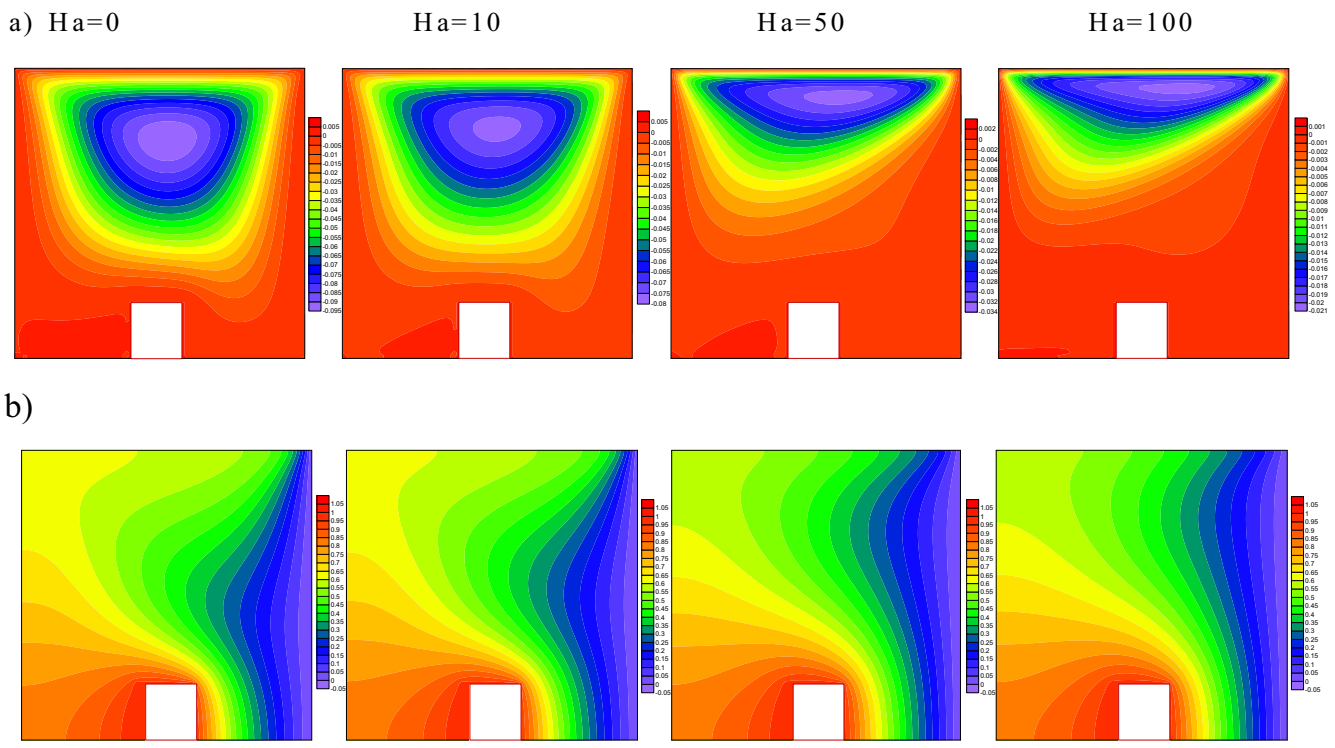

Fig. 12 Various values of Ha on streamlines (top) and isothermal (bottom).

4. Results and discussion

In this section, the present problem is investigated numerically of hot obstacle position on magneto-hybrid nanofluid flow in a lid-driven porous cavity. Except for the differences in the respective figures and tables, these values are considered to be fixed on the entire computation $HA = 10$, $H = 0.2$, $W = 0.2$, $Ri = 10$, $Re = 10$, $D1 = 0.5$, $\Phi = 30^0$, $\varepsilon = 0.02$, $DA = 10^{-2}$, $\gamma_e = 0.02$ respectively. The obtained numerical results characterized by typical streamlines, isotherms, local Nusselt numbers, and average Nusselt numbers for different values of involved parameters including Reynolds number (Re), Richardson number (Ri), non-Darcy (DA), Hartmann number (Ha), position ($D1$), height (H) and a width (W) of the obstacle results of these computations are presented and discussed in the following subsections.

4.1. Position of obstacle ($D1$)

The consequences for changing the different values of the obstacle position over the bottom wall on the distribution of streamlines are exposed in Fig. 3(a). When the square obstacle is changing the positions from 0.3 to 0.7 from the left to right wall of cavity, a top vortex formed inside the cavity and it is moving from the left to right wall of the cavity. There is no significant effect on the behavior of streamlines on changing the position of the obstacle. Fig. 3(b) illustrates the effect of the isotherms in different values of obstacle position. When the square obstacle is placed at positions from 0.3 to 0.7 the cause to decline the thickness of the right wall of the cavity. As a consequence, the temperature decreases in the square cavity. Fig. 4 shows that the influence of the local Nusselt number growth of changing the position of the obstacle illustrates the heat transfer enhancement. The average Nusselt number on changing the position of a hot obstacle increases the heat transfer is shown in Fig. 5.

4.2. Non-Darcy (DA)

The effects of different Darcy numbers on the streamlines are illustrated in Fig. 6(a). Increasing the DA from 10^{-6} to 10^{-2} is a significant effect on the velocity. We observed that the higher

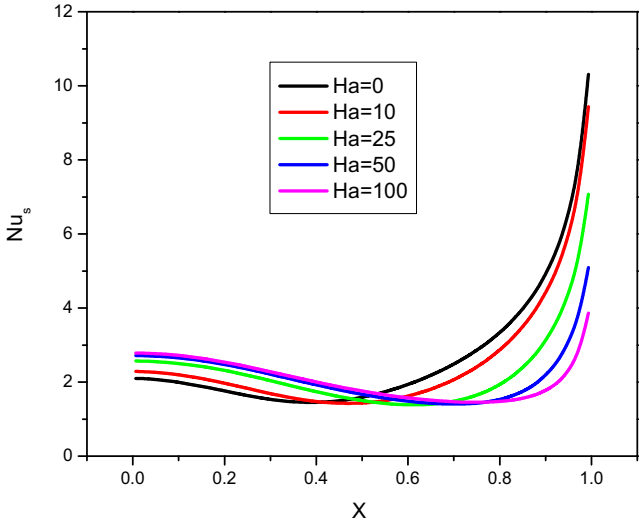

Fig. 13 The effect of different values of Haon the local Nusselt number.

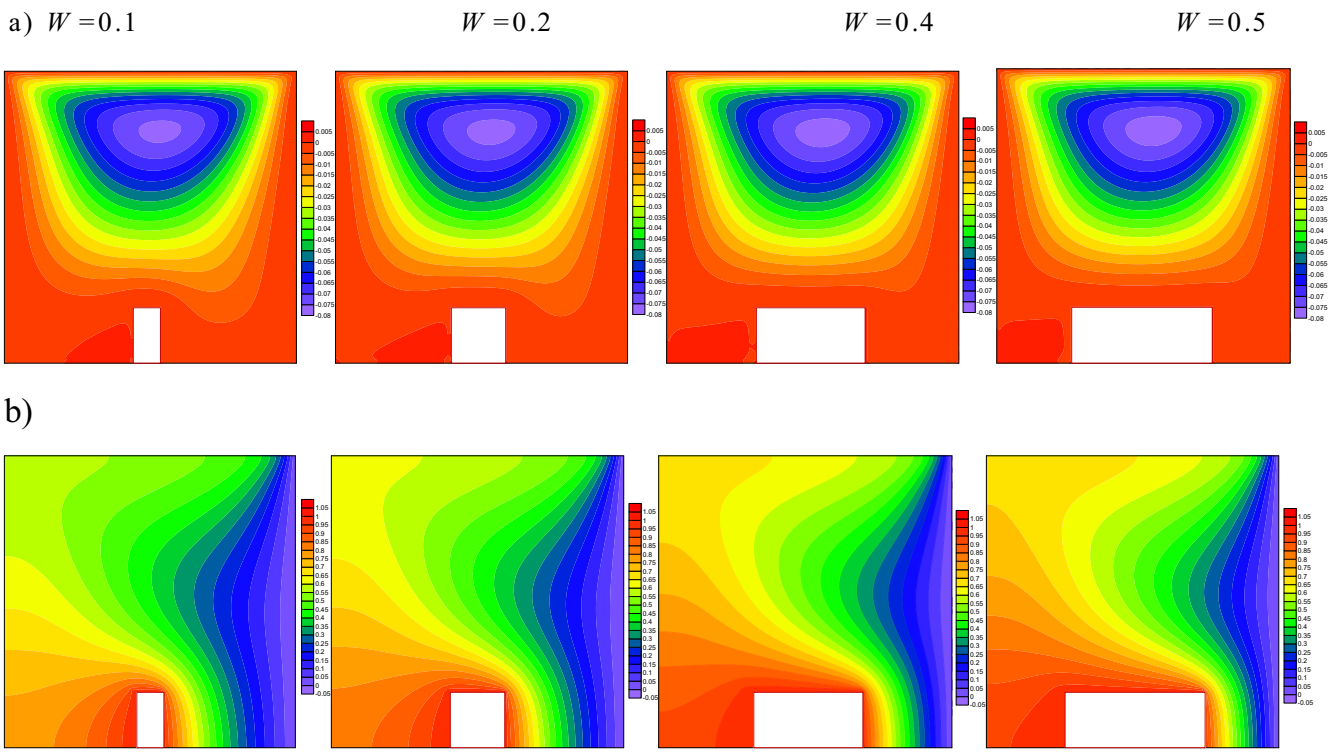

Fig. 14 Various values of W on streamlines (top) and isothermal (bottom).

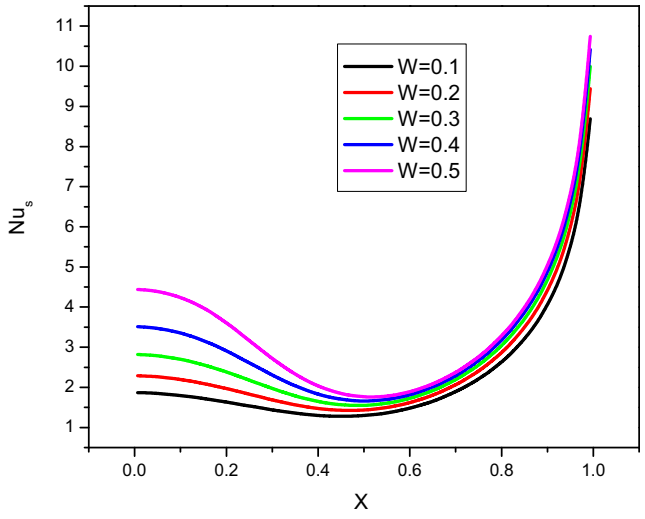

Fig. 15 The effect of W on the local Nusselt number.

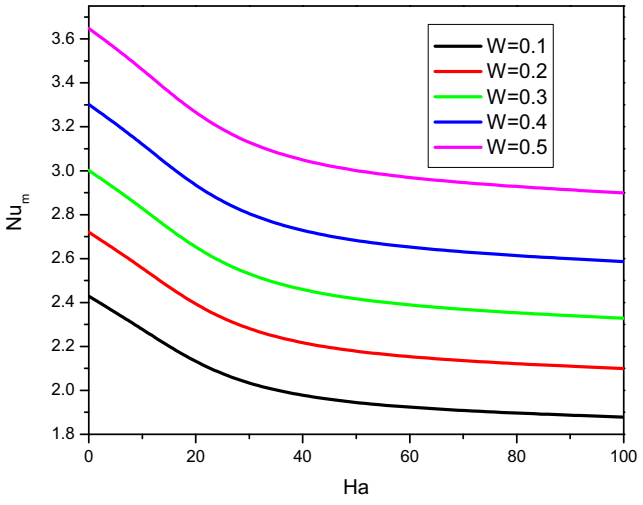

Fig. 16 The effect of W on the average Nusselt number.

values of *DA* increasing the velocity, the streamlines are circulating in the clockwise direction. Fig. 6(b) illustrates the effect of the Isotherms in different values of Darcy numbers. The highest values of Darcy number enhancing the rate of heat transfer. The isothermal lines move around the clockwise direction due to higher heat transfer. The higher Darcy number values increase the velocity of the fluid, and as a result, the square cavity temperature rises. The influence of the several values of the Darcy number on the distribution of local Nusselt number is illustrated in Fig. 7. The low values of the Darcy number declines the rate of heat transfer. The distribution of the average Nusselt number on the hot obstacle for different Darcy numbers is shown in Fig. 8. The higher values of Darcy number increases the heat transfer rate.

4.3. Height of different obstacles (H)

The impact of increasing the height of the obstacle on the streamline is plotted in Fig. 9(a) It is seen from this figure that, when elevates the obstacle height causes the streamlines to circulate in the clockwise direction. Fig. 9(b) presents the influence of isotherms for various values of the obstacle height. Isotherms and rate of heat transfer has highly affected with an increment of obstacle height. Physically, growing the obstacle height causes the right wall of the cavity to flow the heat in

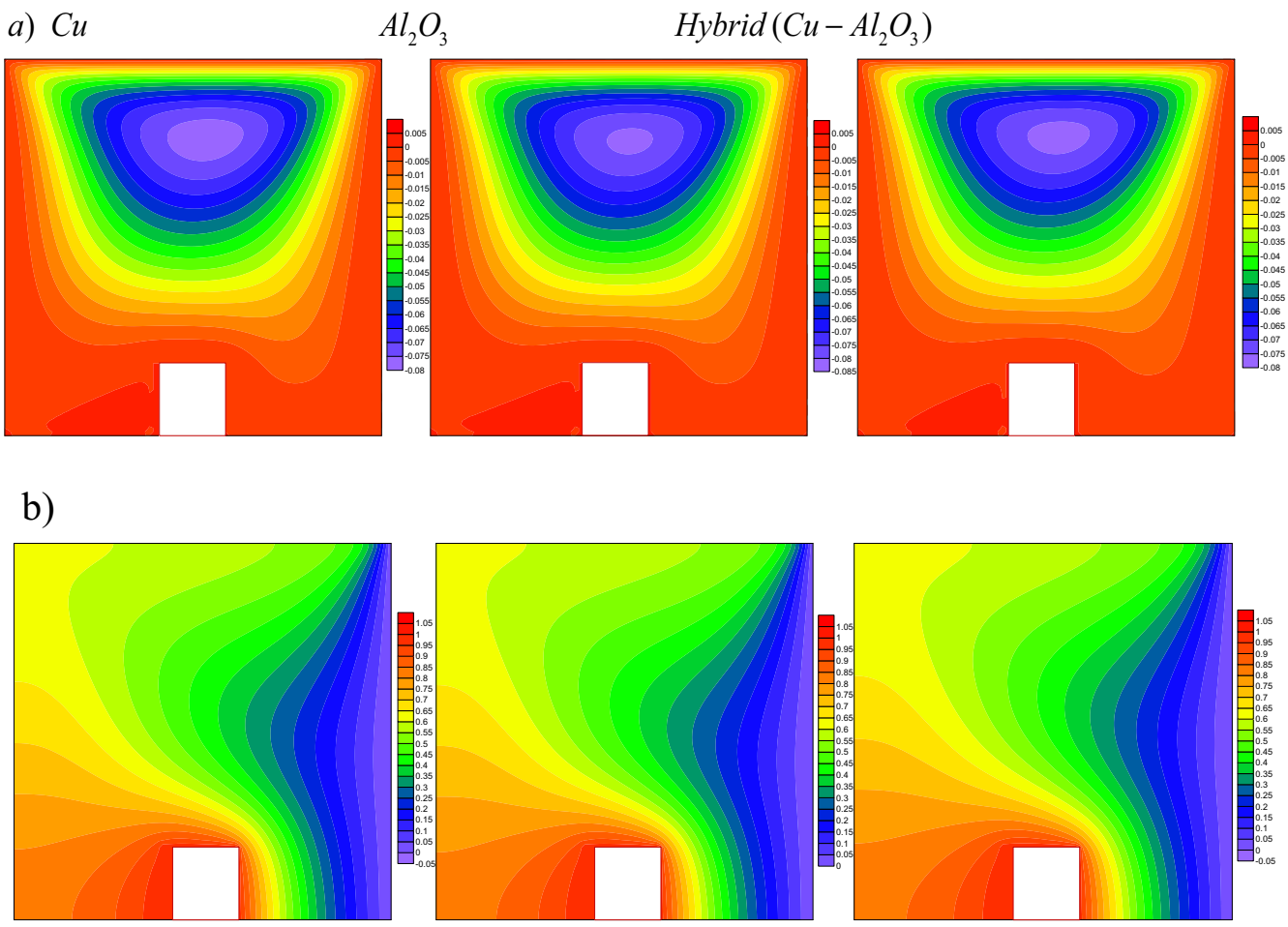

Fig. 17 Various values of *Cu*-water, *Al2O3*-water and Hybrid (*Cu-Al2O3*) nanofluids on streamlines (top) and isothermal (bottom).

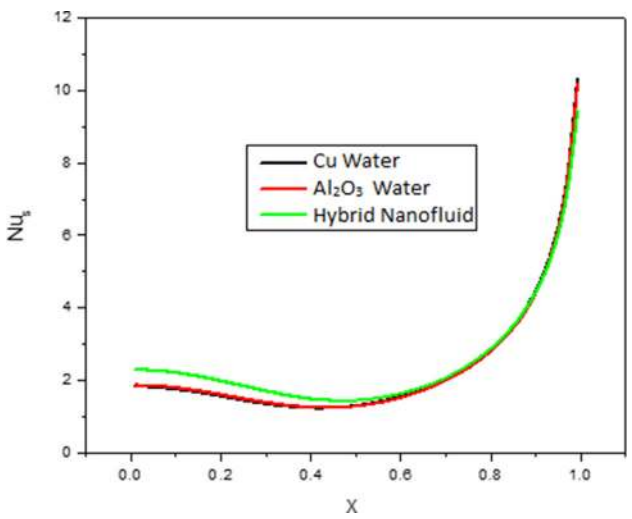

Fig. 18 Variation of *Cu*-water, Al_2O_3-water and Hybrid (*Cu*-Al_2O_3) nanofluids of local Nusselt number.

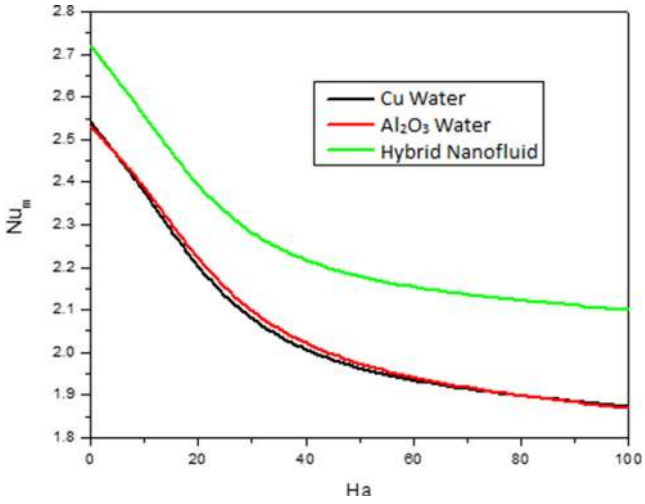

Fig. 19 Variation of *Cu*-water, Al_2O_3-water and Hybrid (*Cu*-Al_2O_3) nanofluids on average Nusselt number.

clockwise direction. Figs. 10 and 11 shows the effect of local and average Nusselt number for the five different heights of a hot obstacle. When increasing the height of the obstacle it enhances the heat transfer.

4.4. Impact of hartman number (Ha)

The consequences for the different values of the Hartmann number on the distribution of streamlines are presented in

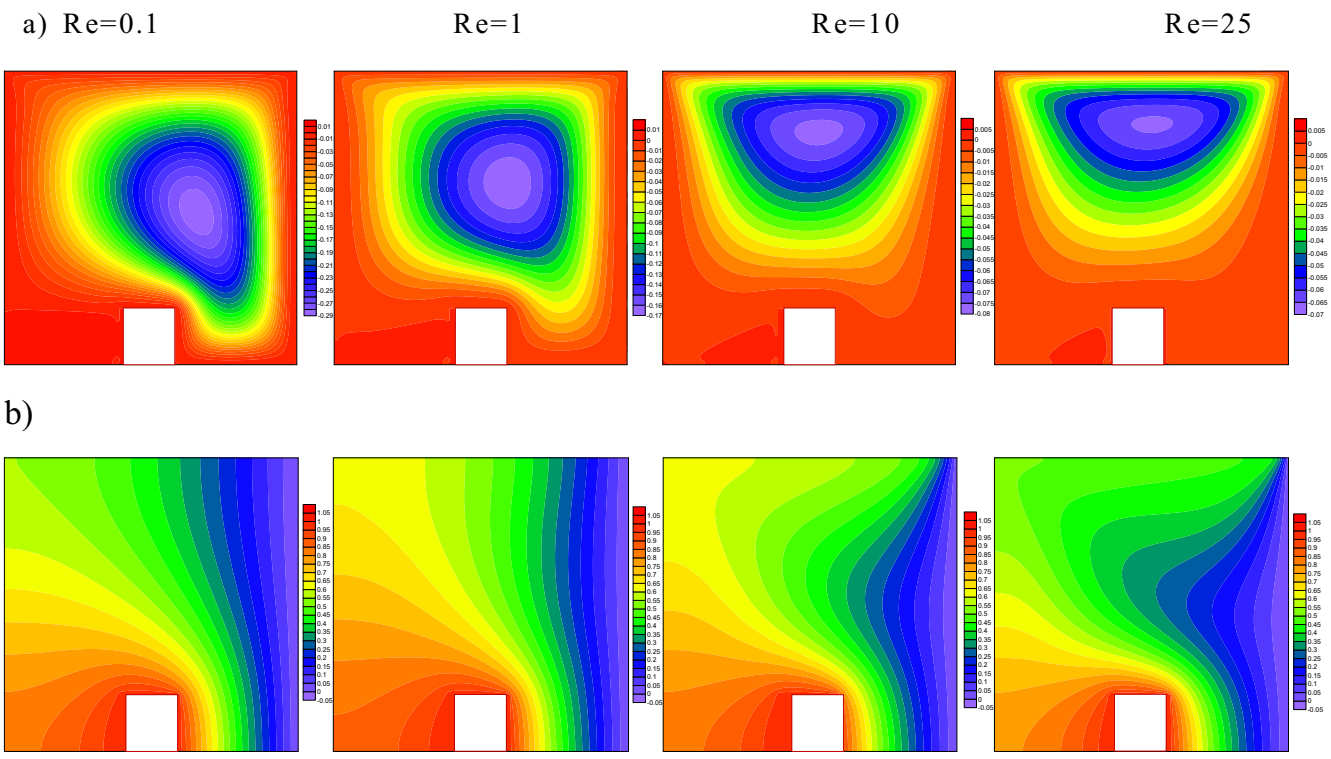

Fig. 20 Various values of *Re* on streamlines (top) and isothermal (bottom).

Fig. 12(a). The vortex moves freely in the square cavity, due to the absence of the magnetic field because the magnetic field opposes the buoyancy force. It is noticed that when increasing the magnetic field from 10 to 100 the streamlines are circulating in the anticlockwise direction in the top portion of the square cavity. This happens as a result of the magnetic field applied in the inclined direction. Fig. 12(b) illustrates the different values of the Hartmann number on the distribution of isotherms. Increasing values of the magnetic field cause to decline in the thickness of the right wall. Physically, a larger magnetic field promotes the temperature as a consequence, the temperature rises in the square cavity. The distribution of the local Nusselt numbers on the heated obstacle for different Ha values are shown in Fig. 13. The higher values of the Ha declines the local Nusselt number.

4.5. Width of the obstacle (W)

Fig. 14(a) shows the effect of streamlines for the different values of the width of the heat obstacle. When increasing the width of the obstacle inside the cavity from 0.1 to 0.5 there is no significant impact on the streamlines. Fig. 14(b) shows the influence of isotherms on the different values of the width of the heat obstacle. Increasing the width of the obstacle cause to decline in the thickness of the right wall, this enhances the heat transfer in the clockwise direction. Variation of obstacle width on local and average Nusselt number is exhibited in Figs. 15 and 16. From these figures, the rate of heat transfer is enhancing due to an increment in the width of the heated obstacle.

4.6. Hybrid nanofluid (Cu-Al_2O_3 -Water)

Fig. 17(a) depicts the effect of two different nanoparticles (*Cu*, Al_2O_3,) in the base fluid (water) on the streamlines. There is no significant effect on the *Cu-water*, Al_2O_3 *-water*, *Cu-*Al_2O_3 / Water (Hybrid nanofluid) in the streamlines, but the strength of streamlines is slightly reduced with nanofluid. Fig. 17(b) shows the effect of isotherms. It is shown that the overall shape of the isotherm contours is the same for both base fluid (water) and hybrid nanofluid (*Cu-*Al_2O_3 /Water) and there is no signif-

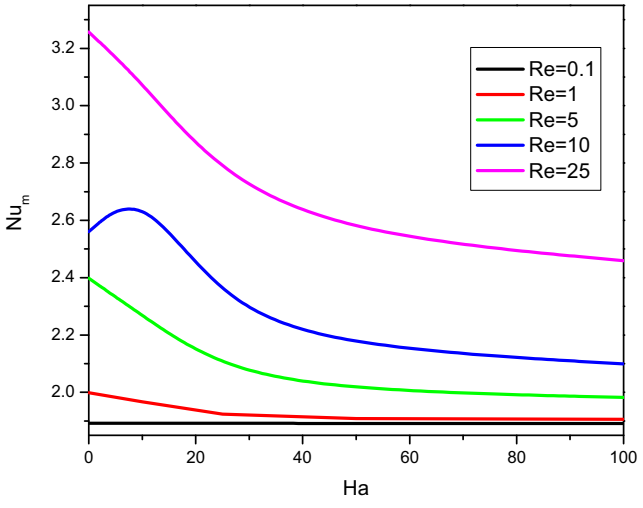

Fig. 21 The effect of *Re* on the average Nusselt number.

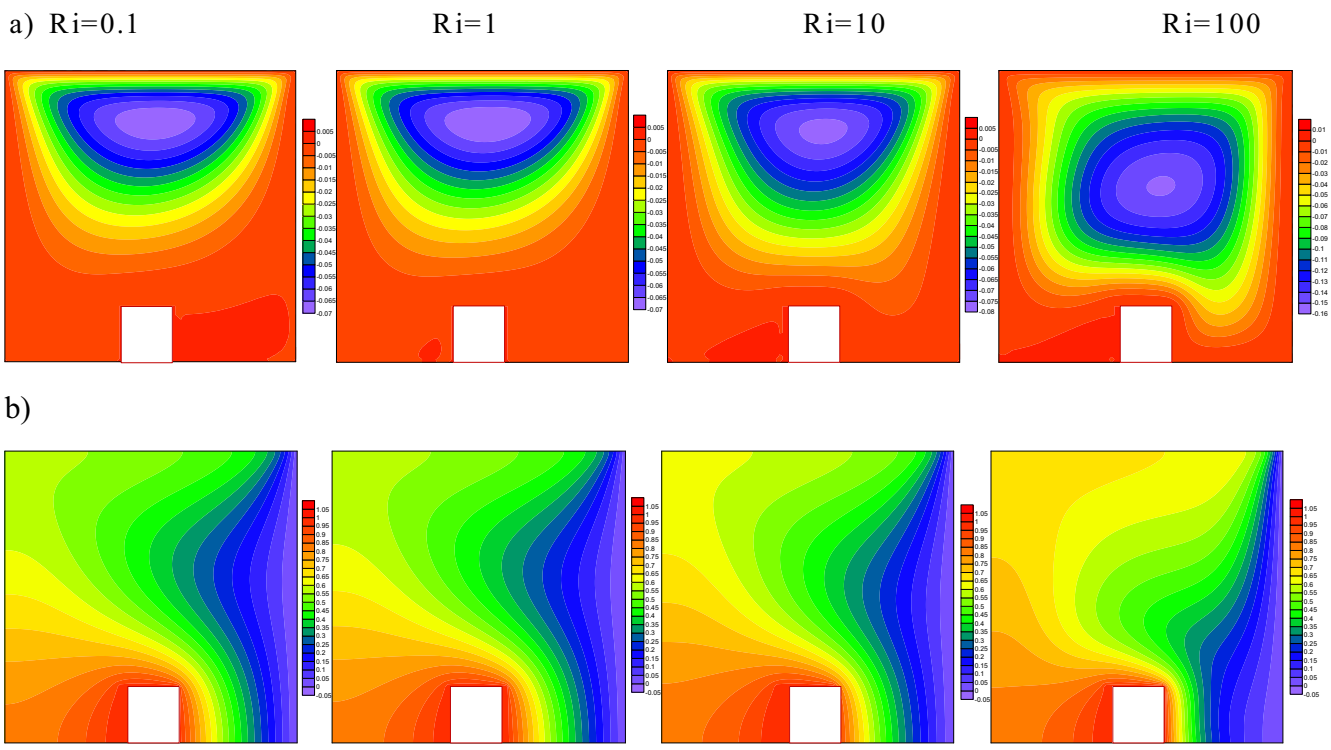

Fig. 22 Various values of *Ri*on streamlines (top) and isothermal (bottom).

icant effect on the rate of heat transfer. Fig. 18 illustrates the influences of Cu-water nanofluid, Al_2O_3 -water nanofluidCu-Al_2O_3/Water hybrid nanofluid on the local Nusselt number. Physically, hybrid nanofluid provides a higher heat transfer rate than the other two nanofluids because of the hybrid nanofluid thermal conductivity is higher than the Cu and Al_2O_3 water nanofluid. In Fig. 19 the average Nusselt number shows hybrid nanofluid thermal conductivity is higher than the Cu and Al_2O_3 water nanofluid.

4.7. Effect of Reynolds number (Re)

Fig. 20(a) illustrates the streamline for the different Reynolds numbers. It is observed that at $Re = 0.1$ the fluid flow of the vortex forms the upper right side of the obstacle in the clockwise direction. An increment of the Reynolds number reflects the growth of the vortex. The highest *Re* value changes the direction of the vortex as an anticlockwise direction. Fig. 20(b) shows the effect of different Reynolds on the isotherms. A rise of Reynolds number cause to decline the thickness of the right wall. Physically, the higher Reynolds number demotes the temperature as a consequence, the temperature decreases in the square cavity. In Fig. 21 shows the higher values of the Re increasing the growth of the average Nusselt number.

4.8. Effect of Richardson (Ri)

The effect of the Richardson numbers on the streamlines shown in Fig. 22(a). The flow pattern shows the forming of a vortex with a circular right side of the cavity in the clockwise direction. When increasing the Richardson number the vortex becomes thicker in the streamlines. Fig. 22(b) demonstrates the different values of Richardson on isotherms. The higher values of the Richardson number increasing the rate of heat transfer. Physically, increasing the Richardson number enhancing the shear stresses, thus growing shear stresses lead to produce resistance to fluid motion and during such resistance heat transfer rises in the square cavity. At the highest Richardson number declines the thickness of the right wall. Fig. 23 illustrates the impact of different Richardson number from 0.01 to 100 in the average Nusselt number. The higher value

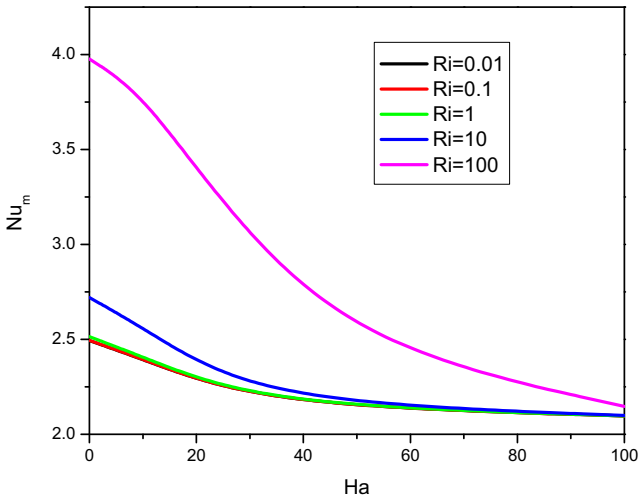

Fig. 23 Variation of *Ri* on the average Nusselt number.

of the *Ri* enhancing the heat transfer and increasing the thermal conduction of the square cavity.

5. Conclusions

Heat transfer derived previously researchers have used Fourier law to define a heat transfer equation, present model, we capture the temperature equation by using non-Fourier heat flux model because Fourier law has a drawback to explain the heat transfer duo thermal relaxation time. Moreover, in the current study, the enhancement of mixed convection flow can be analyzed by the moving of the obstacle in different positions like moves towards the right wall or left wall. To the best of author's knowledge and based on the above literature survey, no studies have reported on hybrid nanofluid (Cu-Al_2O_3/water) flow in a lid-driven non-Darcy porous cavity with Cattaneo-Christov heat flux Pattern. Dimensionless partial differential equations are computed with the use of a finite volume-based simple algorithm. Impacts of active parameters like Richardson number, Hartmann number, and heights of the obstacle, width of the obstacle, Reynolds number, and Darcy number are projected via streamlines, isotherms, local and average Nusselt number. The prime outcome of the present study is listed below:

1. The higher values of Darcy number increases the velocity and heat transfer rate.
2. The hybrid nanofluid thermal conductivity is higher than the Cu and Al_2O_3 water nanofluid.
3. The higher values of the *Ri*enhancing the heat transfer and also increases the thermal conduction of the square cavity.
4. The higher Reynolds number declines the thickness of the right wall and demotes the temperature as a consequence.
5. From this present model, it is exposed that the Cu-Al_2O_3/water nanofluid provides a higher heat transfer.
6. The intensity of fluid flow lessens with an increment of Hartmann number.
7. Increasing values of the Hartmann number cause to decline in the thickness of the right wall and reduce the local Nusselt number.

Declaration of Competing Interest

The authors declare that they have no known competing financial interests or personal relationships that could have appeared to influence the work reported in this paper.

References

[1] S.U.S.S. Choi, Enhancing thermal conductivity of fluids with nanoparticles, Am. Soc. Mech. Eng. Fluids Eng. Div. FED. 231 (1995) 99–105.

[2] K. Hosseinzadeh, A.J. Amiri, S.S. Ardahaie, D.D. Ganji, Effect of variable lorentz forces on nanofluid flow in movable parallel plates utilizing analytical method, Case Stud. Therm. Eng. 10 (2017) 595–610, https://doi.org/10.1016/j.csite.2017.11.001.

[3] M. Sheikholeslami, T. Hayat, A. Alsaedi, MHD free convection of Al2O3-water nanofluid considering thermal radiation: A numerical study, Int. J. Heat Mass Transf. 96 (2016) 513–524, https://doi.org/10.1016/j.ijheatmasstransfer.2016.01.059.

[4] Z. Abdelmalek, S. Ullah Khan, H. Waqas, H.A. Nabwey, I. Tlili, Utilization of second order slip, activation energy and viscous dissipation consequences in thermally developed flow of third grade nanofluid with gyrotactic microorganisms, Symmetry 12 (2) (2020) 309.

[5] S.M. Hashem Zadeh, M. Sabour, S. Sazgara, M. Ghalambaz, Free convection flow and heat transfer of nanofluids in a cavity with conjugate solid triangular blocks: Employing Buongiorno's mathematical model, Phys. A Stat. Mech. Appl. 538 (2020) 122826, https://doi.org/10.1016/j.physa.2019.122826.

[6] K. Hosseinzadeh, A.R. Mogharrebi, A. Asadi, M. Sheikhshahrokhdehkordi, S. Mousavisani, D.D. Ganji, Entropy generation analysis of mixture nanofluid (H2O/c2H6O2)–Fe3O4 flow between two stretching rotating disks under the effect of MHD and nonlinear thermal radiation, Int. J. Ambient Energy. 0750 (2019), https://doi.org/10.1080/01430750.2019.1681294.

[7] M. Ghalambaz, M. Sabour, S. Sazgara, I. Pop, R. Trâmbiţaş, Insight into the dynamics of ferrohydrodynamic (FHD) and magnetohydrodynamic (MHD) nanofluids inside a hexagonal cavity in the presence of a non-uniform magnetic field, J. Magn. Magn. Mater. 497 (2019) 166024, https://doi.org/10.1016/j.jmmm.2019.166024.

[8] I. Tlili, H.A. Nabwey, G.P. Ashwinkumar, N. Sandeep, 3-D magnetohydrodynamic AA7072-AA7075/methanol hybrid nanofluid flow above an uneven thickness surface with slip effect, Sci. Rep. 10 (1) (2020) 1–3.

[9] A.M. Rashad, H.A. Nabwey, Gyrotactic mixed bioconvection flow of a nanofluid past a circular cylinder with convective boundary condition, J. Taiwan Inst. Chem. Eng. 1 (99) (2019) 9–17.

[10] N. Muhammad, S. Nadeem, A. Issakhov, Finite volume method for mixed convection flow of Ag–ethylene glycol nanofluid flow in a cavity having thin central heater, Phys. A Stat. Mech. Appl. 537 (2020) 122738, https://doi.org/10.1016/j.physa.2019.122738.

[11] S.A.M. Mehryan, F.M. Kashkooli, M. Ghalambaz, A.J. Chamkha, Free convection of hybrid Al_2O_3-Cu water nanofluid in a differentially heated porous cavity, Adv. Powder Technol. 28 (2017) 2295–2305, https://doi.org/10.1016/j.apt.2017.06.011.

[12] S.O. Giwa, M. Sharifpur, J.P. Meyer, Experimental study of thermo-convection performance of hybrid nanofluids of Al_2O_3-MWCNT/water in a differentially heated square cavity, Int. J. Heat Mass Transf. 148 (2020) 119072, https://doi.org/10.1016/j.ijheatmasstransfer.2019.119072.

[13] K. Hosseinzadeh, A. Asadi, A.R. Mogharrebi, M.E. Azari, D. D. Ganji, Investigation of mixture fluid suspended by hybrid nanoparticles over vertical cylinder by considering shape factor effect, J. Therm. Anal. Calorim. 25 (2020) 1–5.

[14] M. Gholinia, K. Hosseinzadeh, D.D. Ganji, Investigation of different base fluids suspend by CNTs hybrid nanoparticle over a vertical circular cylinder with sinusoidal radius, Case Stud. Thermal Eng. 29 (2020) 100666.

[15] Z.A. Raizah, A.M. Aly, Natural convection from heated shape in nanofluid-filled cavity using incompressible smoothed particle hydrodynamics, J. Thermophys Heat Transfer 33 (4) (2019) 917–931.

[16] Z.A. Raizah, Natural convection from cross blade inside a nanofluid-filled cavity using ISPH method, Int. J. Numer. Meth. Heat Fluid Flow (2020).

[17] G.H. Kefayati, Mixed convection of non-Newtonian nanofluid in an enclosure using Buongiorno's mathematical model, Int. J. Heat Mass Transf. 1 (108) (2017) 1481–1500.

[18] G.R. Kefayati, FDLBM simulation of mixed convection in a lid-driven cavity filled with non-Newtonian nanofluid in the presence of magnetic field, Int. J. Therm. Sci. 1 (95) (2015) 29–46.

[19] G.R. Kefayati, Mesoscopic simulation of mixed convection on non-Newtonian nanofluids in a two sided lid-driven enclosure, Adv. Powder Technol. 26 (2) (2015) 576–588.
[20] G.R. Kefayati, Mixed convection of non-Newtonian nanofluids flows in a lid-driven enclosure with sinusoidal temperature profile using FDLBM, Powder Technol. 1 (266) (2014) 268–281.
[21] G.R. Kefayati, Magnetic field effect on heat and mass transfer of mixed convection of shear-thinning fluids in a lid-driven enclosure with non-uniform boundary conditions, J. Taiwan Inst. Chem. Eng. 1 (51) (2015) 20–33.
[22] A. Ahmadi Balootaki, A. Karimipour, D. Toghraei, Nano scale lattice Boltzmann method to simulate the mixed convection heat transfer of air in a lid-driven cavity with an endothermic obstacle inside, Phys. A Stat. Mech. Appl. 508 (2018) 681–701, https://doi.org/10.1016/j.physa.2018.05.141.
[23] F. Selimefendigil, Mixed convection in a lid-driven cavity filled with single and multiple-walled carbon nanotubes nanofluid having an inner elliptic obstacle, Propuls. Power Res. 8 (2019) 128–137, https://doi.org/10.1016/j.jppr.2019.01.007.
[24] R. Ellahi, S.M. Sait, N. Shehzad, N. Mobin, Numerical simulation and mathematical modeling of electro-osmotic couette-poiseuille flow of MHD power-law nanofluid with entropy generation, Symmetry (Basel). 11 (2019) 1038, https://doi.org/10.3390/sym11081038.
[25] N. Khan, H.A. Nabwey, M.S. Hashmi, S.U. Khan, I. Tlili, A theoretical analysis for mixed convection flow of Maxwell fluid between two infinite isothermal stretching disks with heat source/sink, Symmetry. 12 (1) (2020) 62.
[26] A.W. Islam, M.A.R. Sharif, E.S. Carlson, Mixed convection in a lid driven square cavity with an isothermally heated square blockage inside, Int. J. Heat Mass Transf. 55 (2012) 5244–5255, https://doi.org/10.1016/j.ijheatmasstransfer.2012.05.032.
[27] A.M. Rashad, M.A. Ismael, A.J. Chamkha, M.A. Mansour, MHD mixed convection of localized heat source/sink in a nanofluid-filled lid-driven square cavity with partial slip, J. Taiwan Inst. Chem. Eng. 68 (2016) 173–186, https://doi.org/10.1016/j.jtice.2016.08.033.
[28] M. Manchanda, K.M. Gangawane, Mixed convection in a two-sided lid-driven cavity containing heated triangular block for non-Newtonian power-law fluids, Int. J. Mech. Sci. 144 (2018) 235–248, https://doi.org/10.1016/j.ijmecsci.2018.06.005.
[29] K.M. Gangawane, MHD Free convection in a partially heated open-ended square cavity: effect of angle of magnetic field and heater location, Int. J. Appl. Comput. Math. 5 (2019) 1–19, https://doi.org/10.1007/s40819-019-0652-9.
[30] A.I. Alsabery, M.A. Ismael, A.J. Chamkha, I. Hashim, Effect of nonhomogeneous nanofluid model on transient natural convection in a non-Darcy porous cavity containing an inner solid body, Int. Commun. Heat Mass Transf. 110 (2020) 104442, https://doi.org/10.1016/j.icheatmasstransfer.2019.104442.
[31] D.J. Krishna, T. Basak, S.K. Das, Natural convection in a non-Darcy anisotropic porous cavity with a finite heat source at the bottom wall, Int. J. Therm. Sci. 48 (2009) 1279–1293, https://doi.org/10.1016/j.ijthermalsci.2008.11.022.
[32] M. Sheikholeslami, M. Sadoughi, Mesoscopic method for MHD nanofluid flow inside a porous cavity considering various shapes of nanoparticles, Int. J. Heat Mass Transf. 113 (2017) 106–114, https://doi.org/10.1016/j.ijheatmasstransfer.2017.05.054.
[33] A.A. Merrikh, A.A. Mohamad, Non-Darcy effects in buoyancy driven flows in an enclosure filled with vertically layered porous media, Int. J. Heat Mass Transf. 45 (2002) 4305–4313, https://doi.org/10.1016/S0017-9310(02)00135-7.
[34] G.H.R. Kefayati, Magnetic field effect on heat and mass transfer of mixed convection of shear-thinning fluids in a lid-driven enclosure with non-uniform boundary conditions, J. Taiwan Inst. Chem. Eng. 51 (2015) 20–33, https://doi.org/10.1016/j.jtice.2015.01.006.
[35] A.K. Rostami, K. Hosseinzadeh, D.D. Ganji, Hydrothermal analysis of ethylene glycol nanofluid in a porous enclosure with complex snowflake shaped inner wall, Waves Random Complex Medium 30 (2020) 1–8.
[36] H.A. Nabwey, H.A. El-Mky, Lie group analysis of thermophoresis on a vertical surface in a porous medium, J. King Saud Univ.-Sci. 31 (4) (2019) 1048–1055.
[37] K. Hosseinzadeh, A. Asadi, A.R. Mogharrebi, J. Khalesi, S. Mousavisani, D.D. Ganji, Entropy generation analysis of (CH2OH) 2 containing CNTs nanofluid flow under effect of MHD and thermal radiation, Case Stud. Thermal Eng. 1 (14) (2019) 100482.
[38] K. Hosseinzadeh, A.R. Mogharrebi, A. Asadi, M. Sheikhshahrokhdehkordi, S. Mousavisani, D.D. Ganji, Entropy generation analysis of mixture nanofluid (H2O/c2H6O2)–Fe3O4 flow between two stretching rotating disks under the effect of MHD and nonlinear thermal radiation, Int. J. Ambient Energy 30 (2019) 1–3.
[39] S. Salehi, A. Nori, K. Hosseinzadeh, D.D. Ganji, Hydrothermal analysis of MHD squeezing mixture fluid suspended by hybrid nanoparticles between two parallel plates, Case Stud. Thermal Eng. 16 (2020) 100650.
[40] I.E. Sarris, S.C. Kakarantzas, A.P. Grecos, N.S. Vlachos, MHD natural convection in a laterally and volumetrically heated square cavity, Int. J. Heat Mass Transf. 48 (2005) 3443–3453, https://doi.org/10.1016/j.ijheatmasstransfer.2005.03.014.
[41] S.R.R. Reddy, P.B.A. Reddy, K. Bhattacharyya, Effect of nonlinear thermal radiation on 3D magneto slip flow of Eyring-Powell nanofluid flow over a slendering sheet with binary chemical reaction and Arrhenius activation energy, Adv. Powder Technol. 30 (2019) 3203–3213, https://doi.org/10.1016/j.apt.2019.09.029.
[42] M. Sheikholeslami, M.M. Rashidi, Effect of space dependent magnetic field on free convection of Fe_3O_4-water nanofluid, J. Taiwan Inst. Chem. Eng. 56 (2015) 6–15, https://doi.org/10.1016/j.jtice.2015.03.035.
[43] K. Hosseinzadeh, S. Roghani, A.R. Mogharrebi, A. Asadi, M. Waqas, D.D. Ganji, Investigation of cross-fluid flow containing motile gyrotactic microorganisms and nanoparticles over a three-dimensional cylinder, Alexandria Eng. J. 59 (2020) 3297–3307, https://doi.org/10.1016/j.aej.2020.04.037.
[44] G.C. Bourantas, V.C. Loukopoulos, MHD natural-convection flow in an inclined square enclosure filled with a micropolar-nanofluid, Int. J. Heat Mass Transf. 79 (2014) 930–944, https://doi.org/10.1016/j.ijheatmasstransfer.2014.08.075.
[45] C.I. Christov, On frame indifferent formulation of the Maxwell-Cattaneo model of finite-speed heat conduction, Mech. Res. Commun. 36 (2009) 481–486, https://doi.org/10.1016/j.mechrescom.2008.11.003.
[46] S.M. Seyyedi, A.S. Dogonchi, M. Hashemi-Tilehnoee, M. Waqas, D.D. Ganji, Entropy generation and economic analyses in a nanofluid filled L-shaped enclosure subjected to an oriented magnetic field, Appl. Therm. Eng. 168 (2020) 114789, https://doi.org/10.1016/j.applthermaleng.2019.114789.
[47] M. Hemmat Esfe, M. Akbari, A. Karimipour, M. Afrand, O. Mahian, S. Wongwises, Mixed-convection flow and heat transfer in an inclined cavity equipped to a hot obstacle using nanofluids considering temperature-dependent properties, Int. J. Heat Mass Transf. 85 (2015) 656–666, https://doi.org/10.1016/j.ijheatmasstransfer.2015.02.009.
[48] M. Rajarathinam, N. Nithyadevi, A.J. Chamkha, Heat transfer enhancement of mixed convection in an inclined porous cavity using Cu-water nanofluid, Adv. Powder Technol. 29 (2018) 590–605, https://doi.org/10.1016/j.apt.2017.11.032.
[49] A.M. Rashad, A.J. Chamkha, M.A. Ismael, T. Salah, Magnetohydrodynamics natural convection in a triangular cavity filled with a Cu-Al_2O_3/water hybrid nanofluid with

localized heating from below and internal heat generation, J. Heat Transfer. 140 (2018), https://doi.org/10.1115/1.4039213.
[50] K.M. Khanafer, A.J. Chamkha, Mixed convection flow in a lid-driven enclosure filled with a fuid-saturated porous medium, Int. J. Heat Mass Transf. 31 (1999) 1354–1370.
[51] R. Iwatsu, J.M. Hyun, K. Kuwahara, Mixed convection in a driven cavity with a stable vertical temperature gradient, Int. J. Heat Mass Transf. 36 (1993) 1601–1608, https://doi.org/10.1016/S0017-9310(05)80069-9.